ACS NANO

www.acsnano.org

ARTICLE

Long-Lived Hot Electron in a Metallic Particle for Plasmonics and Catalysis: *Ab Initio* Nonadiabatic Molecular Dynamics with Machine Learning

Weibin Chu, Wissam A. Saidi,* and Oleg V. Prezhdo*

Cite This: *ACS Nano* 2020, 14, 10608−10615

Read Online

ACCESS | Metrics & More | Article Recommendations | Supporting Information

ABSTRACT: **Multiple experiments provide evidence for photovoltaic, catalytic, optoelectronic, and plasmonic processes involving hot, *i.e.*, high energy, electrons in nanoscale materials. However, the mechanisms of such processes remain elusive, because electrons rapidly lose energy by relaxation through dense manifolds of states. We demonstrate a long-lived hot electron state in a Pt nanocluster adsorbed on the MoS_2 substrate. For this purpose, we develop a simulation technique, combining classical molecular dynamics based on machine learning potentials with *ab initio* nonadiabatic molecular dynamics and real-time time-dependent density functional theory. Choosing Pt_{20}/MoS_2 as a prototypical system, we find frequent shifting of a top atom in the Pt particle occurring on a 50 ps time scale. The distortion breaks particle symmetry and creates unsaturated chemical bonds. The lifetime of the localized state associated with the broken bonds is enhanced by a factor of 3. Hot electrons aggregate near the shifted atom and form a catalytic reaction center. Our findings prove that distortion of even a single atom can have important implications for nanoscale catalysis and plasmonics and provide insights for utilizing machine learning potentials to accelerate *ab initio* investigations of excited state dynamics in condensed matter systems.**

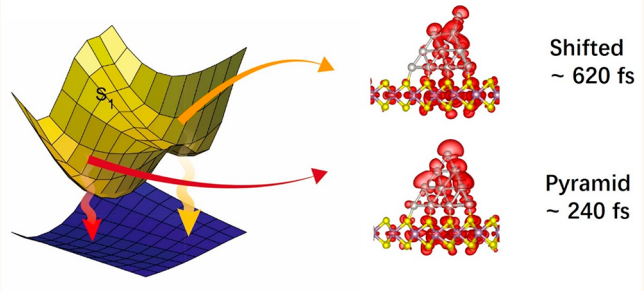

KEYWORDS: *nanoparticle, electron trapping, machine learning, excited state dynamics, time-dependent density functional theory*

Noble metal nanoclusters (NCs) have drawn significant interest in different research fields such as nanoelectronics, energy conversion, and catalysis.[1−6] Studies have shown that NCs have many novel properties, which strongly depend on NC size and shape.[7] For instance, small NCs are catalytically active, exhibiting activity that strongly correlates with exposed edge and corner atoms,[7,8] even for materials that display very limited reactivity in the bulk phase.[9,10] NCs represent a metastable state of matter and are often supported by substrates to prevent cluster coagulation. Substrates, as well as cluster/substrate interfaces, also play an important role in the catalytic activity, for instance, by providing charge carriers and facilitating charge transfer between different parts of a catalytic system.[10,11]

Metal NCs play important roles in solar energy harvesting and utilization, both acting as light harvesters *via* plasmon resonances, and providing photocatalytic sites. Electrons and holes photogenerated in NCs and substrates initiate many chemical reactions. Interfacial charge transfer between NCs and a substrate affects the catalytic activity in competition with other charge carrier processes, such as energy relaxation, diffusion, trapping, and recombination. Charge trapping constitutes an important step in photocatalysis, since it allows charge accumulation at catalytic sites in NCs and prevents recombination of electron−hole pairs.[12,13] Platinum (Pt) clusters are widely used as cocatalysts that are often employed as efficient charge trapping agents in photocatalysis.[14,15]

Plasmonic properties of noble metal NCs are frequently used to accelerate and control chemical reactions.[16−23] Experiments have addressed the importance of localized surface plasmon resonance (LSPR) excitations in plasmonic catalysis.[16,17,21,24] For instance, Mukherjee *et al.* reported that

Received: June 6, 2020
Accepted: July 29, 2020
Published: July 29, 2020

https://dx.doi.org/10.1021/acsnano.0c04736
ACS Nano 2020, 14, 10608−10615

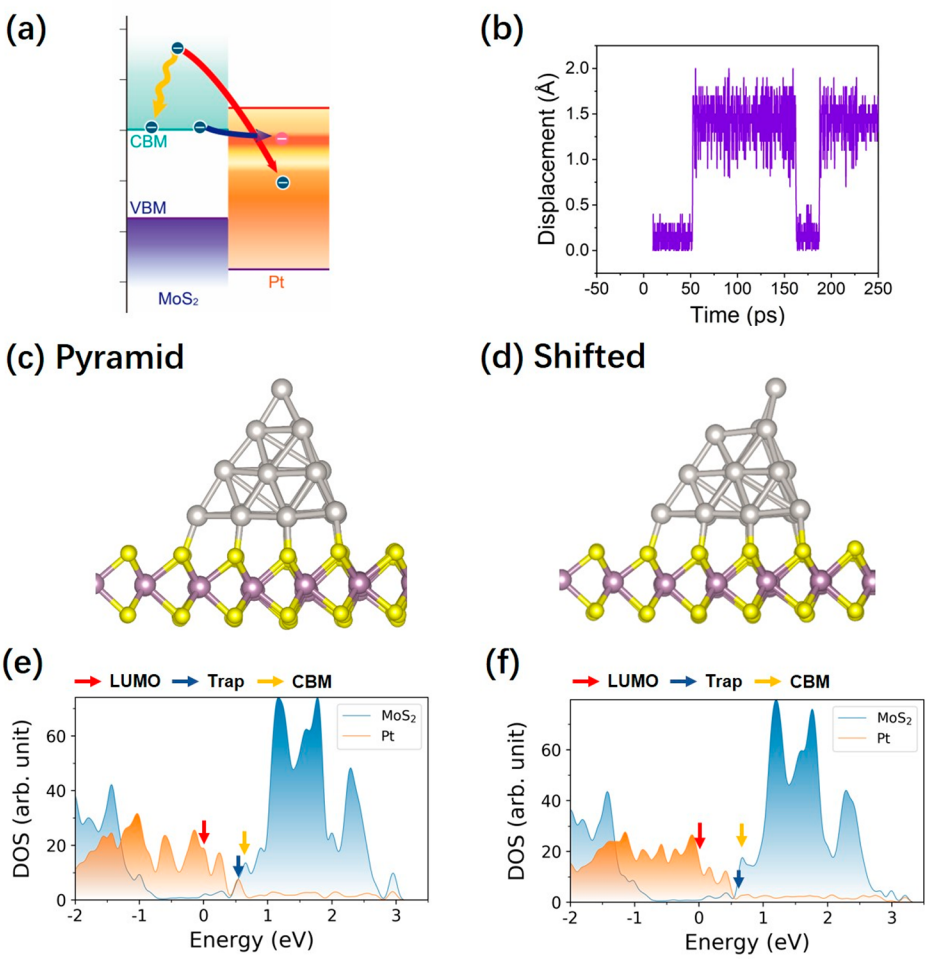

Figure 1. (a) Schematic of hot electron injection and relaxation in the Pt/MoS_2 system. Electrons generated in MoS_2 by light or electricity transfer to the Pt NC. Electrons close to the MoS_2 CBM populate a long-lived trap state in the NC, blue arrow, while higher energy electrons bypass the trap state and relax much more rapidly, orange arrow. (b) Displacement of the top atom of the Pt NC as a function of time in the ML-NAMD simulation. (c, d) Side views of the two distinct configurations, labeled as pyramid and shifted. (e, f) Corresponding density of states (DOS). The zero of energy is set at the Fermi energy. The NC spends significant amounts of time in the local minimum with the displaced top Pt atom, part (d), corresponding to the 1.5 Å displacement relative to pyramid, part (b). The shifted configuration gives rise to long-lived hot electrons and enhanced catalytic activity. The red, blue, and yellow arrows indicate the location of the Pt NC LUMO, the hot electron trap state, and the MoS_2 CBM, respectively.

LSPR in Au nanoparticles decays into hot electrons and triggers H_2 dissociation.[16] Qian *et al.* demonstrated an LSPR-mediated H_2O reduction at Au/TiO_2 heterostructures.[17] Further, it was found that the LSPR can dramatically improve the hydrogen evolution reaction and photoluminescence in Au/MoS_2 hybrids.[19,20]

The molecular and electronic structure of plasmonic NC/semiconductor heterostructures has been investigated at various levels of theory. Previously, we studied the ultrafast electron transfer after plasmon photoexcitation in a Au/TiO_2 system using nonadiabatic molecular dynamics (NAMD).[25] A charge-separated state was found to instantaneously generate after a surface plasmon excitation event, after which the hot electron was fully injected into TiO_2 on a sub-100 fs scale. The theoretical prediction of the instantaneous generation of a charge-separated state was confirmed experimentally one year later.[26] We also studied the plasmon-mediated charge injection from Au particles into MoS_2, at which plasmon-driven charge separation was found to strongly depend on the type of donor−acceptor interaction.[27] However, Au/Ag NCs have limited chemical reactivity that strongly limits their surface reactions through plasmonic catalysis. In contrast, Pt and Pd NCs are much more promising for the design of future devices due to their strong catalytic activities.[28]

Trajectory surface hopping is utilized to study nonadiabatic (NA) electron dynamics by introducing stochastic hops between different potential energy surfaces (PESs).[29,30] One widely used approach is Tully's fewest-switches algorithm.[29] However, surface hopping with *ab initio* generated PESs is challenging in relatively large systems, as it requires long molecular dynamics (MD) trajectories that are computationally expensive. Recently, machine learning (ML) approaches have been shown effective in accelerating first-principles calculations by orders of magnitude without significantly affecting the accuracy of the results.[31−40] While the ML-PESs have been successfully used in ground-state molecular dynamics simulations, the employment of ML in excited state NA dynamics is rare. A few notable recent studies have been reported in this direction by Hu *et al.*[41] and Dral *et al.*[42] These investigations are limited to low-dimensional systems, and it is still challenging to extend them to condensed matter and nanoscale materials with a large number of atoms.

https://dx.doi.org/10.1021/acsnano.0c04736
ACS Nano 2020, 14, 10608−10615

In the past decade, we developed[43−45] a scheme combining NAMD with real-time time-dependent density functional theory (TDDFT) that has shown great success in many fields. Combined with the classical path approximation (CPA),[43,46,47] in which the nuclear dynamics is assumed weakly dependent on the quantum state of the electronic subsystem, as compared to thermal nuclear fluctuations, this approach significantly reduces the computational cost compared to other NAMD and TDDFT methodologies and allows us to study large systems.[48−56] Application of the CPA provides a natural connection to the ML acceleration of MD, allowing us to employ deep learning to greatly enhance the time scale for NAMD and to explore important processes that are not accessible by the traditional means.

In this report, we demonstrate the formation of a long-lived hot electron trap state in a Pt NC adsorbed on MoS_2. The finding is made possible by the technique developed here for simulating *ab initio* quantum dynamics in nanoscale systems, combining ML with NAMD and real-time TDDFT. By investigating the interfacial charge transfer dynamics between the Pt_{20} NC and a MoS_2 monolayer,[7,8] we observe strong distortion of a corner atom of the NC, occurring with every 50−100 ps. Associated with such distortion is the formation of a localized electron trap state that decouples from the rest of the system and extends the hot electron lifetime by a factor of 3. Hot electrons accumulate in this state and create a chemical reaction site. The demonstrated mechanism of hot electron trapping can operate at NC edges, on surfaces containing steps and adatoms, *etc.*, and rationalizes various hot electron chemistries observed in multiple experiments.

RESULTS AND DISCUSSION

We start by investigating the geometric structure and static electronic properties of the system, Figure 1. After the construction of the adiabatic PESs, a 250 ps ML-MD was performed. We have observed two distinct structures in the trajectory, as shown in Figure 1b−d. The structures differ in the location of the NC's top atom. We label the two structures as pyramid and shifted. It is important to emphasize that it is extremely time consuming or even impossible to sample transitions between the two structures using traditional *ab initio* NAMD, and therefore, the uncovered phenomenon of the shifted structure would have not been possible without the developed methodology employed in the current study.

The pyramid structure is very stable in the first 50 ps. However, after that, a significant distortion occurs stabilizing the shifted structure. The corresponding densities of states (DOS) are shown in Figure 1e and f. Despite the variation in the NC morphology, there appear to be no significant differences in the electronic structure between the two configurations. The Pt NC introduces states in the MoS_2 bandgap. Note the peak (blue arrow in Figure 1e,f) located ~0.1 eV below the conduction band minimum (CBM, yellow arrow in Figure 1e,f) of MoS_2. The peak is strongly suppressed when the top Pt atom is shifted. The corresponding orbital distributions show a strong hybridization between the Pt NC and MoS_2 substrate, which could be seen in Figure S2 of the Supporting Information. In the pyramid structure, the peak is attributed to the LUMO+7 and LUMO+8. However, in the shifted structure, the LUMO+7 is much lower in energy than the LUMO+8. The LUMO+8 state, responsible for the suppressed peak in the shifted Pt NC DOS about 0.1 eV below the MoS_2 CBM, Figure 1f, shows a surprising electron trapping ability.

Figure 1a shows a schematic of the simulated charge carrier trapping and relaxation dynamics. Following a photoexcitation of MoS_2, electrons start to relax toward the MoS_2 CBM, as shown by the yellow arrow in Figure 1a. During the relaxation, the hot electron can get injected into the Pt NC, as shown by the red and blue arrows. The schematic matches the calculated DOS, Figure 1e,f, showing that the DOS of the Pt NC at energies above the MoS_2 CBM is low. Figure 1e,f also show that there are a few isolated states near the CBM with strong hybridization between the Pt NC and MoS_2. These states have special properties and can potentially accept the injected hot electron and suppress the subsequent relaxation and recombination inside the metallic Pt NC. Charge trapping in these states can promote the accumulation of hot electrons in the Pt NC and have a significant impact on the NC's photocatalytic activity.

Figure 2 presents the simulation results for hot electron relaxation and trapping for the case in which photoexcitation promotes an electron into the CBM of MoS_2. This situation also describes the scenario in which the electron is excited to energies above the MoS_2 CBM, but far from the NC. This is feasible since in practice the coverge of the metal NCs on MoS_2 is low. In such a case, the electron will relax to the MoS_2 CBM before reaching the NC. Figure 2a characterizes electron injection from MoS_2 to the Pt NC, Figure 2b presents the corresponding energy relaxation curves, while Figure 2c,d show evolving populations of the orbitals.

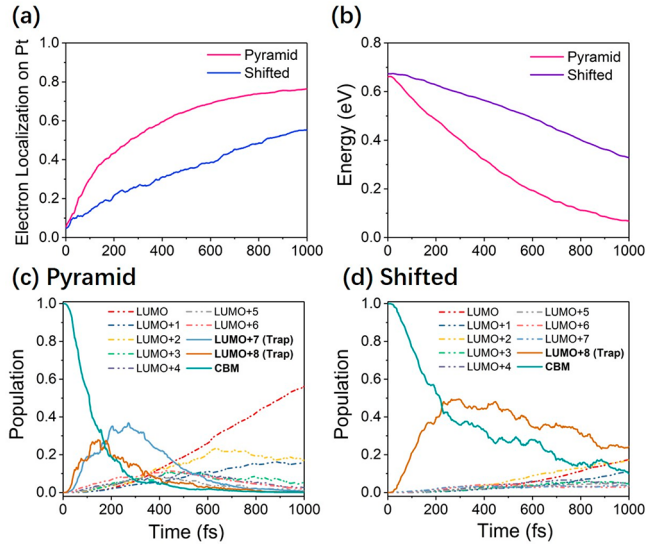

Figure 2. Hot electron injection and relaxation dynamics starting from the CBM of MoS_2. (a) Electron localization on the Pt NC. (b) Electron energy. (c, d) Populations of the relevant orbitals in the pyramid and shifted systems. In the pyramid system, the electron transfers from the MoS_2 CBM to the Pt NC within 200 fs and loses its energy by relaxing to the Fermi level within 1 ps. In the shifted system, the electron transfers to the trap state within 250 fs and has a 30% probability to remain there past 1 ps.

The ML-NAMD results reported in Figure 2a,b demonstrate that both electron injection and energy relaxation are strongly suppressed in the shifted structure compared to the pyramid structure. For the pyramid, around 76% of the electrons are injected into the Pt NC after 1 ps, with an estimated injection

https://dx.doi.org/10.1021/acsnano.0c04736
ACS Nano 2020, 14, 10608−10615

time of 238 fs. By contrast, for the shifted structure, only 55% of the electrons are injected after 1 ps, and the injection time slows down to 617 fs.

To further understand the charge transfer process, we analyzed the electronic populations as functions of time. Figure 2c demonstrates that the hot electron in the pyramid structure quickly transfers to the Pt NC within the first 100 fs and becomes trapped by LUMO+7 and LUMO+8 until 400 fs. These states are strongly hybridized, with significant orbital delocalization in both the Pt NC and MoS_2, Figure S2. We denote these states as electron-trapping states. Figure 2d shows that the injection rate for the shifted structure is comparable with that of the pyramid structure. However, importantly, the time the trapped electrons remain in the LUMO+8 in the shifted configuration is three times longer compared to the pyramid. Moreover, the LUMO+7 in the shifted structure plays no particular role in the hot electron dynamics. The differences in the electron trapping between the two structures arise from the higher symmetry of the pyramid and the stronger hybridization between the Pt NC and MoS_2 in the LUMO+7 and LUMO+8 states of the pyramid. The top atom in the shifted structure reduces the NC symmetry, weakens the hybridization of the LUMO+8, and localizes the electron in the LUMO+7 on the Pt NC, Figure S2.

The enhancement of the hot electron trapping by the distortion of the Pt atom is rationalized by the weaker NA coupling (NAC) between the electron trap state and the unoccupied states of Pt that are lower in energy, as shown in Figure 3. The corresponding average root-mean-square of the

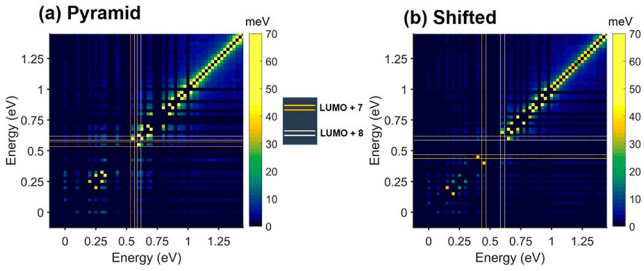

Figure 3. Distribution of average absolute NAC between pairs of electronic states at different energies for (a) pyramid and (b) shifted structures. The zero of energy is set at the Pt LUMO. The LUMO+7 and LUMO+8 are marked with orange and white lines, respectively. The LUMO+8 is the long-lived trap state, Figure 2d. The NAC between a pair of states is larger when the states are closer in energy, *i.e.*, between nearest-neighbor states and in regions of high DOS, Figure 1, or if the states overlap strongly, *i.e.*, with strong hybridization between the substrate and the Pt NC, Figure 4.

NAC is 3.3 meV in the pyramid, which is appreciably larger than 2.1 meV for the shifted structure, as shown in Table 1. In particular, the NAC between the electron trap state and the closest in energy Pt state, which determines the lifetime of the trap state, decreases strongly from 5.7 to 2.9 meV due to the pyramid distortion. The result is consistent with the lowering of the Pt NC symmetry and the weakening of the hybridization between the Pt NC and MoS_2 discussed before. The weaker hybridization also induces a slight decrease of the NAC between the electron trap state and the MoS_2 CBM, from 35.7 to 21.6 meV, Table 1.

The distribution of the electron density for the frontier and electron trapping orbitals further supports the NAC values

Table 1. Root-Mean-Square of Nonadiabatic Coupling (NAC) for the Hot Electron Injection and Trapping Dynamics

	pyramid			shifted		
	trap-LUMO +6[a]	trap-Pt[b]	CBM-trap	trap-LUMO+7	trap-Pt	CBM-trap
NAC (meV)	5.7	3.3	35.7	2.9	2.1	21.6

[a]NAC between the trap state and the Pt state just below it; in the case of the pyramid, it is an average over the two electron trap states. [b]NAC between the trap state and all Pt states below it.

reported in Table 1. The electron densities are depicted in Figure 4 for a typical configuration from the MD trajectory.

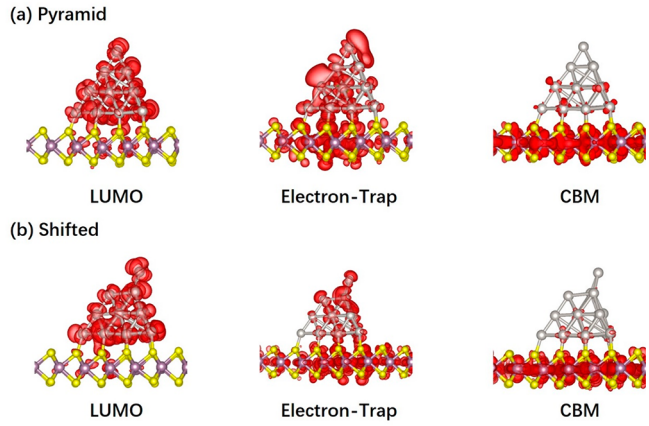

Figure 4. Charge densities of the LUMO, electron trap, and CBM states in the Pt/MoS_2 system for the (a) pyramid and (b) shifted geometries of the Pt NC. The hot electron relaxes from the MoS_2 CBM to the trap state to the Pt NC LUMO. The canonically averaged densities of the electron trapping orbitals are shown in Figure S3. The trap state is shared between the Pt NC and MoS_2. The trapped electron is long-lived in the shifted system, because it is localized on the top Pt atom and is decoupled from the rest of the NC. Note that the trap state is below the MoS_2 CBM, Figure 1, and therefore the electron cannot return to MoS_2.

The canonically averaged densities of the electron trapping orbitals are shown in Figure S3. In both systems, the LUMO of the Pt NC and the CBM of MoS_2 are localized primarily within the corresponding subsystems, while the electron trap state is a strongly hybridized orbital with coupling between the Pt NC and MoS_2 through the Pt−S bond. When the top atom of the pyramid shifts, the electron becomes more localized near the distorted atom. Further, the electron density in the region connecting the Pt NC to MoS_2 is reduced, Figure 4b and Figure S3, decreasing the coupling between the NC and MoS_2. These changes in the orbital distributions decrease the NAC and, consequently, enhance charge trapping.

We further investigated the hot electron relaxation and trapping as a function of excitation energy, by considering three initial electron energies at 1.0, 1.5, and 2.0 eV above the Fermi energy, Figure 5. We found that the nonradiative relaxation accelerates for higher initial energies. This phenomenon can be rationalized by the larger DOS at these energies, Figure 1e,f, and additional relaxation pathways that are not available at lower energies. As demonstrated in detail in Figure 5b−d, only when the electron starts at the MoS_2 CBM does it get trapped in the shifted structure and remains in the

https://dx.doi.org/10.1021/acsnano.0c04736
ACS Nano 2020, 14, 10608−10615

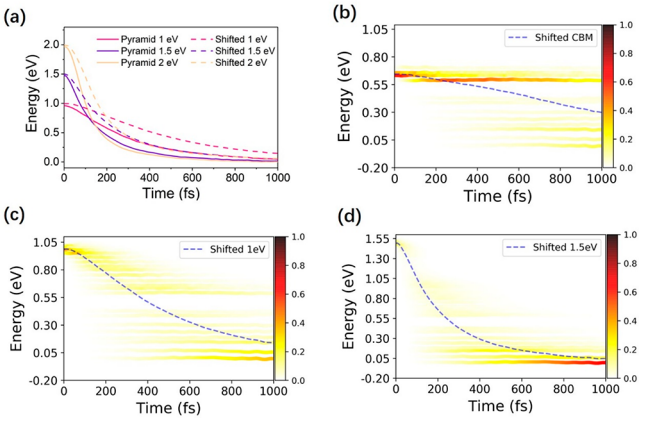

Figure 5. (a) Energy relaxation of hot electrons with different initial energies in the pyramid and shifted systems. Higher initial energy leads to faster relaxation. (b–d) Details of electron relaxation in the shifted system starting at different energies. The color strips show electron distribution over different energy states, and the dashed line represents the average electron energy. The nearly horizontal dark orange line in part (b) demonstrates that the long-lived electron trapping occurs only when the initial electron is close to the MoS_2 CBM.

trap state for a long time. If the electron starts at higher energies, it essentially bypasses the trap state, relaxing directly into the lower energy states of the Pt NC and rapidly reaching the Fermi energy.

Even though the results obtained for high excitation energies appear to be detrimental for the hot electron catalysis, since it is hard to place the electron close to the CBM, the situation is better than it seems. Even if a hot electron is created above the MoS_2 CBM, either by absorption of light, electrically, or chemically, it will rapidly relax to the CBM and will be transported to the Pt NC at the CBM energy. Only if the NC coverage of MoS_2 is high will the hot electron be able to transfer into the NC prior to relaxing to the energy of the MoS_2 CBM. In realistic situations, in which the surface coverage by noble metal particles is moderate or low, the hot electron will be trapped and capable of using its access energy to perform useful chemistry.

The current study assumed that the system is excited at a particular energy. This type of photoexcitation corresponds to sunlight conditions, which are most relevant for solar energy applications. Sunlight can be well approximated as a continuous wavelength radiation or, according to the wave–particle duality, as a stream of photons with particular energies. Because the radiation is continuous, the time approaches infinity, and photons can have well-defined energies, according to the time–energy uncertainty principle. In comparison, light pulses in time-resolved pump–probe laser experiments are short-lived and excite a range of energies. By considering initial conditions at different energies we represent a broad range light spectrum. If electrons reach the Pt particle by transfer from MoS_2, the electrons are already at the MoS_2 CBM, because they decay rapidly through the dense manifold of CB states. If light excites the Pt NC directly, *e.g.*, *via* a surface plasmon resonance, electrons can be generated over a broad range of energies, and the higher energy excitation scenario becomes relevant. The study of the current system indicates that electron transfer from MoS_2 creates more favorable conditions for the charge trapping.

The current simulation focused on a small NC, due to computational limitations. Such particles cannot fully exhibit plasmonic phenomena, although they still show strong light absorption. A similar phenomenon can be expected in plasmonic catalysis as well. The trapping efficiency may decrease in larger NCs, because they contain denser manifolds of electronic states and can exhibit faster electron–phonon relaxation. At the same time, the trapping originates from bond breaking and separation of the top atom from the rest of the pyramid, and this effect should be present for all particle sizes. Similar distortions can happen at NC edges. Surfaces of larger, plasmonic NCs can contain additional atoms that can also act as traps for hot electrons as well. The hot electrons are trapped in our simulations because the NC symmetry is broken, and atoms with unsaturated chemical bonds are created. Such unsaturated bonds give rise to localized states that are decoupled from the rest of the system and exhibit long lifetimes. The bond breaking and decoupling of one or a few atoms from the rest of the system is critical for plasmon-induced charge separation, photocatalysis, and other excited state phenomena observed with metallic particles. The competition between such decoupling and electron–phonon relaxation determines whether the observed effects involve excited electronic states or arise from thermal heating. The demonstrated mechanism of hot electron trapping can operate in many different systems and rationalize various hot electron chemistries.

The findings reported in this work were possible due to a combination of ML and NAMD. Application of the CPA to NAMD[43] allowed us to use ML in order to develop an efficient *ab initio* accuracy force field, to sample a long trajectory, and to uncover an important system geometry giving rise to long-lived hot electron traps. Using ML to obtain excited state force fields is straightforward conceptually, but challenging computationally, since excited state energies and forces are much harder to compute and since one needs to consider many excited states. Using ML to obtain a parametrization for the NAC is even more challenging, because the number of NAC matrix elements grows quadratically with the number of states, the calculation of NAC is more challenging than the force calculation, and NAC dependence on nuclear geometry and velocity is complex. Even under the CPA, NAMD requires NAC calculations. Therefore, our strategy was to sample system geometry using ML and then obtain the NAC using traditional *ab initio* calculations for small parts of the ML trajectory. While we cannot perform NAMD entirely using ML yet, the developed ML-NAMD strategy is practical and computationally affordable, allowing one to study quantum dynamics of excited electrons on picosecond and nanosecond scales and to uncover important and nontrivial regimes. The ML-NAMD with *ab initio* NAC can be used to simulate large systems accurately with significant cost reduction compared to the traditional *ab initio* NAMD.

CONCLUSIONS

To summarize, we have demonstrated a long-lived hot electron state in the Pt NC adsorbed on the MoS_2 substrate. Existence of such states can rationalize many experimental findings on hot electron transfer in plasmonics, as well as photo- and electron-chemical catalysis. The finding has been made possible by the development of the *ab initio* quantum dynamics methodology, combining ML-MD, NAMD, and real-time TDDFT. Trained to *ab initio* calculations, ML-MD allows

https://dx.doi.org/10.1021/acsnano.0c04736
ACS Nano 2020, 14, 10608–10615

one to obtain long trajectories and sample rare events. The unusual quantum dynamics that accompany such events are modeled by real-time TDDFT for electrons coupled to atomic motions *via* NAMD. The top atom of the pyramid-like NC shifts frequently during a hundreds of picosecond ML-MD simulation. *Ab initio* TDDFT/NAMD modeling of the hot electron relaxation shows strong electron trapping when the top atom of the pyramid NC is shifted. Mechanistic analysis indicates that this geometric distortion suppresses coupling between the NC and the substrate and that the electrons aggregate to the shifted atom, forming a reaction center. We propose that hot electron reaction centers created by such distortions can operate in different NCs and other nanoscale systems and constitute an important consideration for the rational design of functional materials for optoelectronic and catalytic applications.

METHODOLOGY

We utilize a deep neural network to describe atomic interactions in the Pt/MoS_2 system as generated using DeepPOT-SE.[57] Briefly, the training set for the ML potential has been generated using CP2K[58] in conjunction with MOLOPT basis sets[59] and GTH norm-conserving pseudopotentials.[60] We have used different systems in the training of the potential, including pristine MoS_2, bulk Pt, Pt (100), (110), and (111) surfaces, isolated Pt clusters, and Pt clusters supported on a MoS_2 substrate.[61−63] Additional details are provided in the Supporting Information and ref 64. The *ab initio* NAMD simulations are performed using the Pyxaid code[43,44] within the TDDFT framework similar to ref 45 in conjunction with the Vienna *ab initio* simulation package (VASP).[65−67] The electron−nuclear interactions are described using the projector augmented wave (PAW) method.[68] We use the Perdew−Burke−Ernzerhof (PBE)[69] exchange−correlation functional in conjunction with the DFT-D3 van der Waals correction.[70] We represent monolayer MoS_2 using a 6×6 supercell and sample the Brillouin zone at the Γ-point. The NAMD phase consistency problem is corrected using a method similar to ref 71. The reported results of the *ab initio* quantum dynamics simulations are obtained by averaging over an ensemble of 5×10^5 realizations of NAMD. The ensemble is generated starting from 50 different initial configurations, with each configuration giving rise to 1×10^4 NAMD trajectories. The ML-MD starts from a pyramid-shaped Pt_{20} NC. The initial Pt_{20}/MoS_2 configuration is determined from a combined theoretical and experimental approach, with the structure obtained first with a genetic algorithm utilizing adaptive atomistic force fields and DFT and then validated using aberration-corrected scanning transmission electron microscopy.[8,61] A 250 ps MD trajectory is generated with the ML force field. Then, *ab initio* NAMD is carried out based on the ML-MD trajectories for representative pyramid and shifted configurations.

ASSOCIATED CONTENT

Supporting Information

The Supporting Information is available free of charge at https://pubs.acs.org/doi/10.1021/acsnano.0c04736.

Details of training of machine-learning force field, test of its performance, and charge densities of key orbitals (PDF)

AUTHOR INFORMATION

Corresponding Authors

Oleg V. Prezhdo − *Departments of Chemistry, and Physics and Astronomy, University of Southern California, Los Angeles, California 90089, United States;* orcid.org/0000-0002-5140-7500; Email: prezhdo@usc.edu

Wissam A. Saidi − *Department of Mechanical Engineering and Materials Science, University of Pittsburgh, Pittsburgh, Pennsylvania 15261, United States;* orcid.org/0000-0001-6714-4832; Email: alsaidi@pitt.edu

Author

Weibin Chu − *Departments of Chemistry, and Physics and Astronomy, University of Southern California, Los Angeles, California 90089, United States;* orcid.org/0000-0001-5951-0337

Complete contact information is available at: https://pubs.acs.org/10.1021/acsnano.0c04736

Notes

The authors declare no competing financial interest.

ACKNOWLEDGMENTS

W.C. and O.V.P. acknowledge support of the U.S. National Science Foundation (Award No. CHE-1900510). W.A.S. acknowledges financial support from the U.S. National Science Foundation (Award Nos. DMR-1809085 and CSSI-2003808). The computational work is supported by the University of Southern California Center for High-Performance Computing and the University of Pittsburgh Center for Research Computing through the resources provided.

REFERENCES

(1) Lewis, L. N. Chemical Catalysis by Colloids and Clusters. *Chem. Rev.* **1993**, *93*, 2693−2730.

(2) Neumann, O.; Urban, A. S.; Day, J.; Lal, S.; Nordlander, P.; Halas, N. J. Solar Vapor Generation Enabled by Nanoparticles. *ACS Nano* **2013**, *7*, 42−49.

(3) Grzelczak, M.; Vermant, J.; Furst, E. M.; Liz-Marzan, L. M. Directed Self-Assembly of Nanoparticles. *ACS Nano* **2010**, *4*, 3591−3605.

(4) Farmer, J. A.; Campbell, C. T. Ceria Maintains Smaller Metal Catalyst Particles by Strong Metal-Support Bonding. *Science* **2010**, *329*, 933−936.

(5) Bell, A. T. The Impact of Nanoscience on Heterogeneous Catalysis. *Science* **2003**, *299*, 1688−1691.

(6) Manjavacas, A.; Liu, J. G.; Kulkarni, V.; Nordlander, P. Plasmon-Induced Hot Carriers in Metallic Nanoparticles. *ACS Nano* **2014**, *8*, 7630−7638.

(7) Narayanan, R.; El-Sayed, M. A. Shape-Dependent Catalytic Activity of Platinum Nanoparticles in Colloidal Solution. *Nano Lett.* **2004**, *4*, 1343−1348.

(8) Yang, T. T.; Tan, T. L.; Saidi, W. A. High Activity toward the Hydrogen Evolution Reaction on the Edges of Mos2-Supported Platinum Nanoclusters Using Cluster Expansion and Electrochemical Modeling. *Chem. Mater.* **2020**, *32*, 1315−1321.

(9) Valden, M.; Lai, X.; Goodman, D. W. Onset of Catalytic Activity of Gold Clusters on Titania with the Appearance of Nonmetallic Properties. *Science* **1998**, *281*, 1647−1650.

(10) Chen, M. S.; Goodman, D. W. The Structure of Catalytically Active Gold on Titania. *Science* **2004**, *306*, 252−255.

(11) Tauster, S. J.; Fung, S. C.; Garten, R. L. Strong Metal-Support Interactions - Group-8 Noble-Metals Supported on Tio2. *J. Am. Chem. Soc.* **1978**, *100*, 170−175.

(12) Linsebigler, A. L.; Lu, G. Q.; Yates, J. T. Photocatalysis on Tio2 Surfaces - Principles, Mechanisms, and Selected Results. *Chem. Rev.* **1995**, *95*, 735−758.
(13) Dong, C.; Lian, C.; Hu, S.; Deng, Z.; Gong, J.; Li, M.; Liu, H.; Xing, M.; Zhang, J. Size-Dependent Activity and Selectivity of Carbon Dioxide Photocatalytic Reduction over Platinum Nanoparticles. *Nat. Commun.* **2018**, *9*, 1252.
(14) Li, R.; Zhang, F.; Wang, D.; Yang, J.; Li, M.; Zhu, J.; Zhou, X.; Han, H.; Li, C. Spatial Separation of Photogenerated Electrons and Holes among {010} and {110} Crystal Facets of Bivo4. *Nat. Commun.* **2013**, *4*, 1432.
(15) Manzi, A.; Simon, T.; Sonnleitner, C.; Doeblinger, M.; Wyrwich, R.; Stern, O.; Stolarczyk, J. K.; Feldmann, J. Light-Induced Cation Exchange for Copper Sulfide Based Co2 Reduction. *J. Am. Chem. Soc.* **2015**, *137*, 14007−14010.
(16) Mukherjee, S.; Libisch, F.; Large, N.; Neumann, O.; Brown, L. V.; Cheng, J.; Lassiter, J. B.; Carter, E. A.; Nordlander, P.; Halas, N. J. Hot Electrons Do the Impossible: Plasmon-Induced Dissociation of H-2 on Au. *Nano Lett.* **2013**, *13*, 240−247.
(17) Qian, K.; Sweeny, B. C.; Johnston-Peck, A. C.; Niu, W.; Graham, J. O.; DuChene, J. S.; Qiu, J.; Wang, Y.-C.; Engelhard, M. H.; Su, D.; Stach, E. A.; Wei, W. D. Surface Plasmon-Driven Water Reduction: Gold Nanoparticle Size Matters. *J. Am. Chem. Soc.* **2014**, *136*, 9842−9845.
(18) Christopher, P.; Xin, H.; Linic, S. Visible-Light-Enhanced Catalytic Oxidation Reactions on Plasmonic Silver Nanostructures. *Nat. Chem.* **2011**, *3*, 467−472.
(19) Shi, Y.; Wang, J.; Wang, C.; Zhai, T. T.; Bao, W. J.; Xu, J. J.; Xia, X. H.; Chen, H. Y. Hot Electron of Au Nanorods Activates the Electrocatalysis of Hydrogen Evolution on Mos2 Nanosheets. *J. Am. Chem. Soc.* **2015**, *137*, 7365−7370.
(20) Najmaei, S.; Mlayah, A.; Arbouet, A.; Girard, C.; Leotin, J.; Lou, J. Plasmonic Pumping of Excitonic Photoluminescence in Hybrid Mos2-Au Nanostructures. *ACS Nano* **2014**, *8*, 12682−12689.
(21) Brongersma, M. L.; Halas, N. J.; Nordlander, P. Plasmon-Induced Hot Carrier Science and Technology. *Nat. Nanotechnol.* **2015**, *10*, 25−34.
(22) Zhou, L. A.; Martirez, J. M. P.; Finzel, J.; Zhang, C.; Swearer, D. F.; Tian, S.; Robatjazi, H.; Lou, M. H.; Dong, L. L.; Henderson, L.; Christopher, P.; Carter, E. A.; Nordlander, P.; Halas, N. J. Light-Driven Methane Dry Reforming with Single Atomic Site Antenna-Reactor Plasmonic Photocatalysts. *Nat. Energy* **2020**, *5*, 61−70.
(23) Halas, N. J.; Lal, S.; Chang, W. S.; Link, S.; Nordlander, P. Plasmons in Strongly Coupled Metallic Nanostructures. *Chem. Rev.* **2011**, *111*, 3913−3961.
(24) Zhang, Y. C.; He, S.; Guo, W. X.; Hu, Y.; Huang, J. W.; Mulcahy, J. R.; Wei, W. D. Surface-Plasmon-Driven Hot Electron Photochemistry. *Chem. Rev.* **2018**, *118*, 2927−2954.
(25) Long, R.; Prezhdo, O. V. Instantaneous Generation of Charge-Separated State on Tio2 Surface Sensitized with Plasmonic Nanoparticles. *J. Am. Chem. Soc.* **2014**, *136*, 4343−4354.
(26) Wu, K.; Chen, J.; McBride, J. R.; Lian, T. Efficient Hot-Electron Transfer by a Plasmon-Induced Interfacial Charge-Transfer Transition. *Science* **2015**, *349*, 632−635.
(27) Zhang, J.; Guan, M. X.; Lischner, J.; Meng, S.; Prezhdo, O. V. Coexistence of Different Charge-Transfer Mechanisms in the Hot-Carrier Dynamics of Hybrid Plasmonic Nanomaterials. *Nano Lett.* **2019**, *19*, 3187−3193.
(28) Kumar, R.; Sharma, A.; Kaur, M.; Husale, S. Pt-Nanostrip-Enabled Plasmonically Enhanced Broad Spectral Photodetection in Bilayer Mos2. *Adv. Opt. Mater.* **2017**, *5*, 1700009.
(29) Tully, J. C. Molecular-Dynamics with Electronic-Transitions. *J. Chem. Phys.* **1990**, *93*, 1061−1071.
(30) Barbatti, M. Nonadiabatic Dynamics with Trajectory Surface Hopping Method. *Wiley Interdiscip. Rev.: Comput. Mol. Sci.* **2011**, *1*, 620−633.
(31) Behler, J.; Parrinello, M. Generalized Neural-Network Representation of High-Dimensional Potential-Energy Surfaces. *Phys. Rev. Lett.* **2007**, *98*, 146401.
(32) Chen, J.; Xu, X.; Zhang, D. H. Communication: An Accurate Global Potential Energy Surface for the Oh Plus Co -> H + Co2 Reaction Using Neural Networks. *J. Chem. Phys.* **2013**, *138*, 221104.
(33) Behler, J. Constructing High-Dimensional Neural Network Potentials: A Tutorial Review. *Int. J. Quantum Chem.* **2015**, *115*, 1032−1050.
(34) Botu, V.; Ramprasad, R. Adaptive Machine Learning Framework to Accelerate *Ab Initio* Molecular Dynamics. *Int. J. Quantum Chem.* **2015**, *115*, 1074−1083.
(35) Li, Z. W.; Kermode, J. R.; De Vita, A. Molecular Dynamics with On-The-Fly Machine Learning of Quantum-Mechanical Forces. *Phys. Rev. Lett.* **2015**, *114*, No. 096405.
(36) Behler, J. Perspective: Machine Learning Potentials for Atomistic Simulations. *J. Chem. Phys.* **2016**, *145*, 170901.
(37) Jiang, B.; Li, J.; Guo, H. Potential Energy Surfaces from High Fidelity Fitting of *Ab Initio* Points: The Permutation Invariant Polynomial - Neural Network Approach. *Int. Rev. Phys. Chem.* **2016**, *35*, 479−506.
(38) Brockherde, F.; Vogt, L.; Li, L.; Tuckerman, M. E.; Burke, K.; Muller, K. R. Bypassing the Kohn-Sham Equations with Machine Learning. *Nat. Commun.* **2017**, *8*, 872.
(39) Chmiela, S.; Tkatchenko, A.; Sauceda, H. E.; Poltavsky, I.; Schutt, K. T.; Muller, K. R. Machine Learning of Accurate Energy-Conserving Molecular Force Fields. *Sci. Adv.* **2017**, *3*, No. e1603015.
(40) Shen, L.; Yang, W. T. Molecular Dynamics Simulations with Quantum Mechanics/Molecular Mechanics and Adaptive Neural Networks. *J. Chem. Theory Comput.* **2018**, *14*, 1442−1455.
(41) Hu, D. P.; Xie, Y.; Li, X. S.; Li, L. Y.; Lan, Z. G. Inclusion of Machine Learning Kernel Ridge Regression Potential Energy Surfaces in On-The-Fly Nonadiabatic Molecular Dynamics Simulation. *J. Phys. Chem. Lett.* **2018**, *9*, 2725−2732.
(42) Dral, P. O.; Barbatti, M.; Thiel, W. Nonadiabatic Excited-State Dynamics with Machine Learning. *J. Phys. Chem. Lett.* **2018**, *9*, 5660−5663.
(43) Akimov, A. V.; Prezhdo, O. V. The Pyxaid Program for Non-Adiabatic Molecular Dynamics in Condensed Matter Systems. *J. Chem. Theory Comput.* **2013**, *9*, 4959−4972.
(44) Akimov, A. V.; Prezhdo, O. V. Advanced Capabilities of the Pyxaid Program: Integration Schemes, Decoherenc:E Effects, Multi-excitonic States, and Field-Matter Interaction. *J. Chem. Theory Comput.* **2014**, *10*, 789−804.
(45) Craig, C. F.; Duncan, W. R.; Prezhdo, O. V. Trajectory Surface Hopping in the Time-Dependent Kohn-Sham Approach for Electron-Nuclear Dynamics. *Phys. Rev. Lett.* **2005**, *95*, 163001.
(46) Long, R.; Prezhdo, O. V.; Fang, W. H. Nonadiabatic Charge Dynamics in Novel Solar Cell Materials. *Wiley Interdiscip. Rev.: Comput. Mol. Sci.* **2017**, *7*, 29.
(47) Wang, L. J.; Akimov, A.; Prezhdo, O. V. Recent Progress in Surface Hopping: 2011−2015. *J. Phys. Chem. Lett.* **2016**, *7*, 2100−2112.
(48) Chu, W. B.; Zheng, Q. J.; Prezhdo, O. V.; Zhao, J. Co2 Photoreduction on Metal Oxide Surface Is Driven by Transient Capture of Hot Electrons: *Ab Initio* Quantum Dynamics Simulation. *J. Am. Chem. Soc.* **2020**, *142*, 3214−3221.
(49) Li, W.; Vasenko, A. S.; Tang, J. F.; Prezhdo, O. V. Anharmonicity Extends Carrier Lifetimes in Lead Halide Perovskites at Elevated Temperatures. *J. Phys. Chem. Lett.* **2019**, *10*, 6219−6226.
(50) Long, R.; Prezhdo, O. V. Dopants Control Electron-Hole Recombination at Perovskite-Tio2 Interfaces: *Ab Initio* Time-Domain Study. *ACS Nano* **2015**, *9*, 11143−11155.
(51) Lu, T. F.; Wang, Y. S.; Tomko, J. A.; Hopkins, P. E.; Zhang, H. X.; Prezhdo, O. V. Control of Charge Carrier Dynamics in Plasmonic Au Films by Tiox Substrate Stoichiometry. *J. Phys. Chem. Lett.* **2020**, *11*, 1419−1427.
(52) Tong, C. J.; Li, L. Q.; Liu, L. M.; Prezhdo, O. V. Synergy between Ion Migration and Charge Carrier Recombination in Metal-Halide Perovskites. *J. Am. Chem. Soc.* **2020**, *142*, 3060−3068.

https://dx.doi.org/10.1021/acsnano.0c04736
ACS Nano 2020, 14, 10608−10615

(53) Wang, L. J.; Long, R.; Prezhdo, O. V. Time-Domain *Ab Initio* Modeling of Photoinduced Dynamics at Nanoscale Interfaces. *Annu. Rev. Phys. Chem.* **2015**, *66*, 549−579.
(54) Yang, Y. T.; Fang, W. H.; Benderskii, A.; Long, R.; Prezhdo, O. V. Strain Controls Charge Carrier Lifetimes in Monolayer Wse2: *Ab Initio* Time Domain Analysis. *J. Phys. Chem. Lett.* **2019**, *10*, 7732−7739.
(55) Zhou, G. Q.; Cen, C.; Wang, S. Y.; Deng, M. S.; Prezhdo, O. V. Electron-Phonon Scattering Is Much Weaker in Carbon Nanotubes Than in Graphene Nanoribbons. *J. Phys. Chem. Lett.* **2019**, *10*, 7179−7187.
(56) Chu, W. B.; Saidi, W. A.; Zheng, Q. J.; Xie, Y.; Lan, Z. G.; Prezhdo, O. V.; Petek, H.; Zhao, J. Ultrafast Dynamics of Photongenerated Holes at a Ch3oh/Tio2 Rutile Interface. *J. Am. Chem. Soc.* **2016**, *138*, 13740−13749.
(57) Zhang, L. F.; Han, J. Q.; Wang, H.; Saidi, W. A.; Car, R.; E, W. N. End-To-End Symmetry Preserving Inter-Atomic Potential Energy Model for Finite and Extended Systems. *Adv. Neural. Inf. Process. Syst.* **2018**, *31*, 4436−4446.
(58) VandeVondele, J.; Krack, M.; Mohamed, F.; Parrinello, M.; Chassaing, T.; Hutter, J. Quickstep: Fast and Accurate Density Functional Calculations Using a Mixed Gaussian and Plane Waves Approach. *Comput. Phys. Commun.* **2005**, *167*, 103−128.
(59) VandeVondele, J.; Hutter, J. Gaussian Basis Sets for Accurate Calculations on Molecular Systems in Gas and Condensed Phases. *J. Chem. Phys.* **2007**, *127*, 114105.
(60) Goedecker, S.; Teter, M.; Hutter, J. Separable Dual-Space Gaussian Pseudopotentials. *Phys. Rev. B: Condens. Matter Mater. Phys.* **1996**, *54*, 1703.
(61) Shi, Y. L.; Song, B.; Shahbazian-Yassar, R.; Zhao, J.; Saidi, W. A. Experimentally Validated Structures of Supported Metal Nanoclusters on Mos2. *J. Phys. Chem. Lett.* **2018**, *9*, 2972−2978.
(62) Saidi, W. A. Density Functional Theory Study of Nucleation and Growth of Pt Nanoparticles on Mos2(001) Surface. *Cryst. Growth Des.* **2015**, *15*, 642−652.
(63) Saidi, W. A. Trends in the Adsorption and Growth Morphology of Metals on the Mos2(001) Surface. *Cryst. Growth Des.* **2015**, *15*, 3190−3200.
(64) Andolina, C. M.; Williamson, P.; Saidi, W. A. Optimization and Validation of a Deep Learning Cuzr Atomistic Potential: Robust Applications for Crystalline and Amorphous Phases with Near-Dft Accuracy. *J. Chem. Phys.* **2020**, *152*, 11.
(65) Kresse, G.; Hafner, J. *Ab Initio* Molecular-Dynamics for Liquid-Metals. *Phys. Rev. B: Condens. Matter Mater. Phys.* **1993**, *47*, 558.
(66) Kresse, G.; Hafner, J. *Ab Initio* Molecular-Dynamics for Open-Shell Transition-Metals. *Phys. Rev. B: Condens. Matter Mater. Phys.* **1993**, *48*, 13115.
(67) Kresse, G.; Hafner, J. *Ab Initio* Molecular-Dynamics Simulation of the Liquid-Metal Amorphous-Semiconductor Transition in Germanium. *Phys. Rev. B: Condens. Matter Mater. Phys.* **1994**, *49*, 14251.
(68) Kresse, G.; Joubert, D. From Ultrasoft Pseudopotentials to the Projector Augmented-Wave Method. *Phys. Rev. B: Condens. Matter Mater. Phys.* **1999**, *59*, 1758.
(69) Perdew, J. P.; Burke, K.; Ernzerhof, M. Generalized Gradient Approximation Made Simple. *Phys. Rev. Lett.* **1996**, *77*, 3865.
(70) Grimme, S.; Antony, J.; Ehrlich, S.; Krieg, H. A Consistent and Accurate *Ab Initio* Parametrization of Density Functional Dispersion Correction (Dft-D) for the 94 Elements H-Pu. *J. Chem. Phys.* **2010**, *132*, 154104.
(71) Akimov, A. V. A Simple Phase Correction Makes a Big Difference in Nonadiabatic Molecular Dynamics. *J. Phys. Chem. Lett.* **2018**, *9*, 6096−6102.

https://dx.doi.org/10.1021/acsnano.0c04736
ACS Nano 2020, 14, 10608−10615